REPORT DOCUMENTATION PAGE

Public Reporting burden for this collection of information is estimated to average 1 hour per response, including the time for reviewing instructions, searching existing data sources, gathering and maintaining the data needed, and completing and reviewing the collection of information. Send comment regarding this burden estimates or any other aspect of this collection of information, including suggestions for reducing this burden, to Washington Headquarters Services, Directorate for information Operations and Reports, 1215 Jefferson Davis Highway, Suite 1204, Arlington, VA 22202-4302, and to the Office of Management and Budget, Paperwork Reduction Project (0704-0188,) Washington, DC 20503.

1. AGENCY USE ONLY (Leave Blank)	2. REPORT DATE August 31, 2002	3. REPORT TYPE AND DATES COVERED Final Progress Report – 7/1/99-6/30/02

4. TITLE AND SUBTITLE Materials and Modulators for True # Dimensional Displays	5. FUNDING NUMBERS G DAD19-99-1-0220
6. AUTHOR(S) Michael Bass, Alexandra Rapaport, and Nabeel Riza	$DAAD19-99-1-0220$

7. PERFORMING ORGANIZATION NAME(S) AND ADDRESS(ES) School of Optics/CREOL – University of Central Florida 4000 Central Florida Blvd. Orlando, FL 32816-2700	8. PERFORMING ORGANIZATION REPORT NUMBER Final Progress Report – UCF Acct. #65-02-550

9. SPONSORING / MONITORING AGENCY NAME(S) AND ADDRESS(ES) U. S. Army Research Office P.O. Box 12211 Research Triangle Park, NC 27709-2211	10. SPONSORING / MONITORING AGENCY REPORT NUMBER 38886-EL .1

11. SUPPLEMENTARY NOTES
    The views, opinions and/or findings contained in this report are those of the author(s) and should not be construed as an official Department of the Army position, policy or decision, unless so designated by other documentation.

12 a. DISTRIBUTION / AVAILABILITY STATEMENT Approved for public release; distribution unlimited.	12 b. DISTRIBUTION CODE

13. ABSTRACT (Maximum 200 words)

The research conducted in this program primarily concerned identification of materials that would serve in scalable real time 3D displays. Such materials would have to experience two photon absorption of two different wavelength near infrared beams of light only at the intersection of the two beams. Upon such excitation the material would have to emit visible light. Our focus on scalable materials led us to study organic dyes dissolved in polymeric hosts.

Additional research evolved out of the effort above In which we studied 2D displays based on up-conversion of near infrared light in rare earth doped crystalline particles dispersed in a polymeric host. This involved fluoride and orthophosphate crystals doped with Yb^{3+} ions as donor ions and Er^{3+}, Ho^{3+} or Tm^{3+} as acceptor ions.

Some research was carried out to explore unique modulation and scanning schemes based on liquid crystal devices.

14. SUBJECT TERMS 3 dimensional displays, dye doped polymers, rare earth doped crystals, optical scanners			15. NUMBER OF PAGES 35
			16. PRICE CODE

17. SECURITY CLASSIFICATION OR REPORT UNCLASSIFIED	18. SECURITY CLASSIFICATION ON THIS PAGE UNCLASSIFIED	19. SECURITY CLASSIFICATION OF ABSTRACT UNCLASSIFIED	20. LIMITATION OF ABSTRACT UL

NSN 7540-01-280-5500

FINAL PROGRESS REPORT

MATERIALS AND MODULATORS FOR 3D DISPLAYS
GRANT NUMBER: DAAD199910220
TO

DEPARTMENT OF THE ARMY
ARMY RESEARCH OFFICE
P. O. BOX 12211
RESEARCH TRIANGLE PARK, NC 27709-2211

BY:
MICHAEL BASS
SCHOOL OF OPTICS/CREOL
UNIVERSITY OF CENTRAL FLORIDA
ORLANDO, FL 32816

AUGUST, 2002

TABLE OF CONTENTS

LIST OF APPENDIXES, ILLUSTRATIONS AND TABLES

ILLUSTRATIONS:

TABLES

STATEMENT OF THE PROBLEM STUDIED

The research conducted in this program primarily concerned identification of materials that would serve in scalable real time 3D displays. Such materials would have to experience two photon absorption of two different wavelength near infrared beams of light only at the intersection of the two beams. Upon such excitation the material would have to emit visible light. Our focus on scalable materials led us to study organic dyes dissolved in polymeric hosts.

Additional research evolved out of the effort above in which we studied 2D displays based on up-conversion of near infrared light in rare earth doped crystalline particles dispersed in a polymeric host. This involved fluoride and orthophosphate crystals doped with Yb^{3+} ions as donor ions and Er^{3+}, Ho^{3+} or Tm^{3+} as acceptor ions.

Some research was carried out to explore unique modulation and scanning schemes based on liquid crystal devices.

SUMMARY OF THE MOST IMPORTANT RESULTS

We have researched materials and modulators necessary for making true 3D displays. This required exploring the use of dye doped polymers as scalable media in which visible light can be excited by simultaneous absorption of two infrared beams only in the volume of their intersection. This process has been demonstrated and very important features of a 3D display investigated in our current research. We have studied the two photon excitation spectrum of dyes in solution and found that it is unlike the single photon excitation spectrum. In addition, the visible light generated was found to depend on the relative polarization of the two exciting beams. Understanding such features enables us to maximize the choices of wavelengths and polarizations that will excite the strongest visible emission.

We have shown that the strength of emission in the volume element where the two beams overlap is very strongly dependent on the distribution of light in each beam. Besides enabling optimization of 3D displays this knowledge has enabled us to explain how data storage systems employing two different wavelength two photon processes can be made with much improved storage density.

A small side effort grew out of our 3D display work into a very important additional aspect of this program. We had several samples of crystals doped with both Yb^{3+} and another rare earth ion. We knew that by pumping with near infrared light into the Yb^{3+} system of these crystals, energy would be transferred to the other rare earth ion that then emitted visible light. Having shown strong red, green and blue emitters using, respectively, Er^{3+}, Er^{3+} or Ho^{3+}, and Tm^{3+} ions as the co-dopant we reported on the concept of using crystallites of such materials dispersed in a polymeric host as an optically written 2D display. Such a display would employ a diode laser beam for excitation eliminating the use of electron beams, high voltage, and vacuum containers associated with cathode ray tube displays. The optically written 2D display would also be much lighter and, with proper optics, smaller that a comparable CRT.

Our work on modulators for 3D displays led to the development of a new scanner design technology called " Multiplexed Optical Scanner Technology" or MOST. The polarization multiplexed optical scanner or P-MOS has been patented. [1] The theoretical foundations of the wavelength multiplexed optical scanner (W-MOS) were published. [2] Initial experimental work has successfully demonstrated the W-MOS with a 15 degree angular one dimensional scan with 145 scan spots, 1.875 cm scan aperture, and a one nanosecond potential scanning speed.

During the period of this research we received DURIP support for the dual parametric oscillator system required. The system has been received and is in use. Together with the computer controlled spectroscopic and dynamic properties monitoring equipment we employ this system has made our work much more effective than ever. The results obtained for dye excitation spectra and the polarization dependence of the excitation were obtained with this system. We also use this system for dynamics studies in the rare earth doped crystals.

Materials for True 3 D Displays:

This aspect of our research program was designed to understand the process of exciting visible emission through the absorption of two different wavelengths of light by a material. If neither beam of light could excite such emission by itself but the two together would then this process would allow volumetrically selective excitation in the region where the two beams intersected. We call this two photon absorption (induced) emission or TPA/E. The emitting volume would be the volume element (voxel) in a true 3 D display. The concept is sketched in Fig. 1. Prior to our work such a process had been reported in materials that could not be scaled up in size to enable reasonable 3 D displays. [3] We concentrated on materials that could be scaled up in size either through their own low cost or by dispersing emitting particulates in an inexpensive passive host medium. The first type of material, one that can be reasonably scaled up to practical sized displays, is exemplified by the dye doped plastics that we reported previously. [4] Fig. 2 is an intensity profile in false color obtained with a laser beam analyzer of a voxel in 10^{-3} M coumarin 7 in ethanol. This voxel was excited by simultaneous absorption of two photons, one at 750 nm and the other at 1040 nm. In this example the short wavelength beam is able to very weakly excite visible emission through two photon absorption. This appears as the faint vertical blue line in the image. Where the two pump beams intersect and excite visible emission the intensity is 10 to 12 times higher.

Voxel capable of emitting visible light due to TPA/E is excited when both excitation wavelengths are incident

Modulated and scanned light from appropriate optical system and modulators (scanners) at two different wavelengths, one wavelength in each beam path.

Medium capable of TPA/E visible light emission
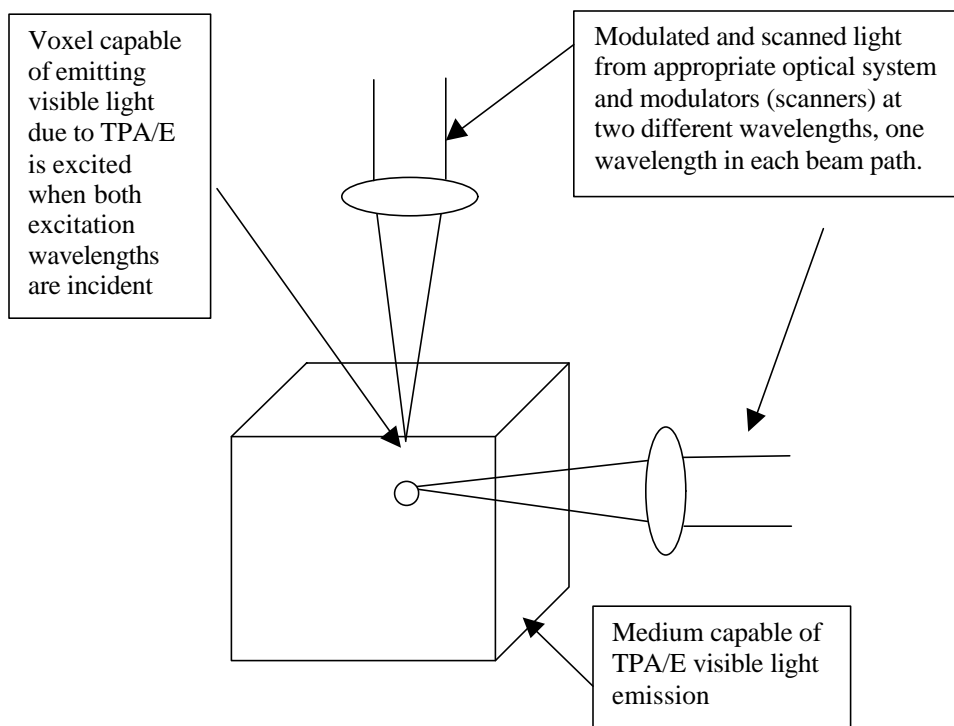
Figure 1. Schematic of 3D display employing TPA/E.
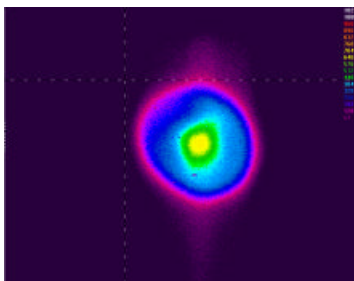
Figure 2. A false color image showing the intensity contours of visible light emitted from a voxel upon TPA/E by two intersecting beams of near infrared light (750 and 1040 nm) in 10^{-3} M coumarin 7 in ethanol.

Initially we expected the two photon excitation spectrum of a dye to be very similar to the linear absorption spectrum so we sought dyes with absorption features that suggested conveniently available excitation wavelengths. For example, one wavelength with second harmonic shorter than, and one with second harmonic longer than the absorption feature but with a sum frequency that would lie within the one photon absorption feature. In our experiments we found that most dyes have absorption spectra that extend beyond the short wavelength side of the primary absorption band. Thus, the short wavelength light could generally excite very weak visible emission through two photon absorption. The long wavelength light never did. However, the two photon excitation spectrum of some dyes is quite different from their one photon spectrum. This is demonstrated by the data in Fig. 3 in which the two spectra for 10^{-3} M rhodamine B in ethanol are shown. Notice that the feature that is a smooth single band in one photon appears as structured in two photon excitation and the feature near 420 nm observed in two photon excitation is not present in one photon. The two peaks in the two photon spectrum can be fit by two Lorentzian curves. These spectra indicate that in the rhodamine B molecule the states involved in one photon absorption have mixed angular momenta but primarily differ by one unit of angular momentum. However, when exciting using two photons it is possible to access a second excited state that has the same angular momentum as the ground state and which is not allowed in a one photon process. In the case of courmarin 7 the two photon and one photon spectra are very similar suggesting that the ground and first excited state are both mixtures of angular momentum states.

Rhodamine B in Ethylene-Glycol
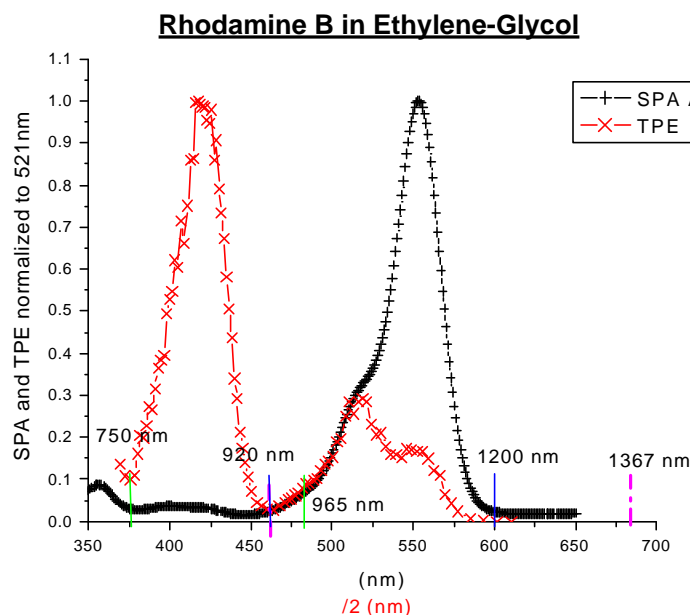
Figure 3. Comparison of one and two photon absorption spectra of 10^{-3} M rhodamine B in ethylene glycol. The black crosses indicate the one photon spectrum and the red x's the two photon absorption plotted at one half the actual wavelength. The green blue and purple tick marks indicate excitation wavelengths used in the polarization studies in Fig. 10.

In the course of our research we observed that the emission strength of the visible light generated by TPA/E was strongly dependent on the relative orientation of the polarizations of the two light beams. It was maximum when the polarizations were parallel and minimum when they were perpendicular to each other. The experiment in which this was studied is sketched in Fig. 4.

As shown in Fig. 5 this dependence is described by a $\cos^2$ function of the angle between the polarizations and the ratio of the maximum to minimum signal is 3. The data in Fig. 5 is for 10^{-3} M rhodamine B in ethanol using two different wavelength pump beams, neither of which experiences two photon absorption alone, to excite the emission by TPA/E. At first, it seems that the polarization dependence is not determined by the dye used as the same polarization dependence is seen for coumarin 7 using non degenerate excitation. When the two beams are set at the same wavelength such that each experiences two photon absorption (a condition of degenerate two photon absorption) there is a similar polarization dependence to the visible light emission.

9
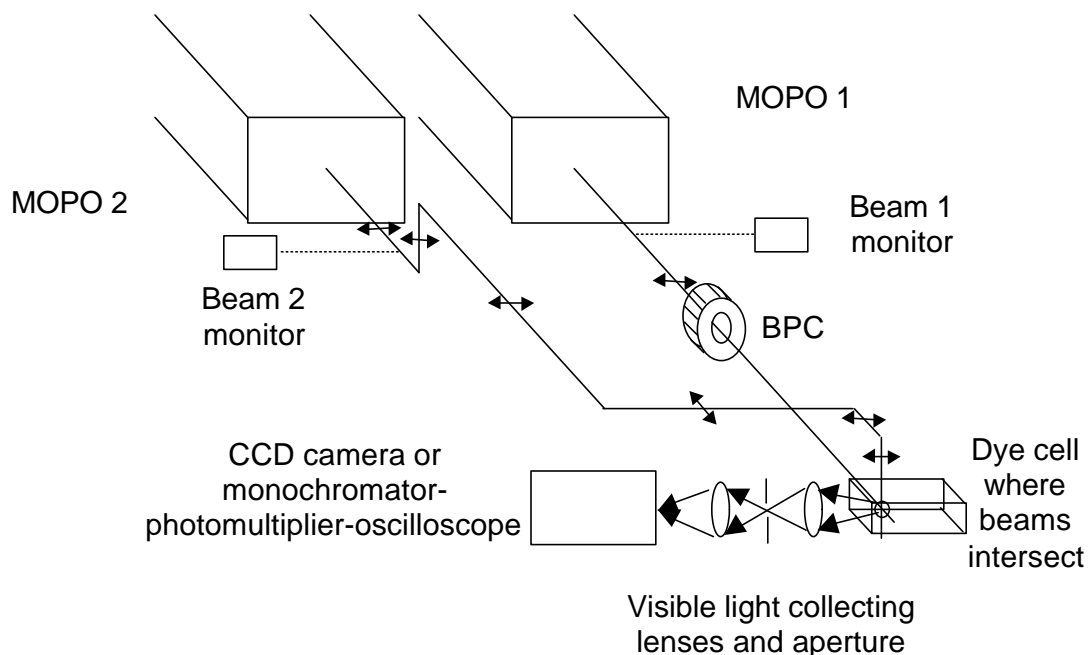
Figure 4. Sketch of experiment in which the effect of the relative angles between the polarizations of the two intersecting beams on two photon absorption was studied. BCP stands for Berek polarization compensator, a device that allowed us to rotate the polarization of beam 1.
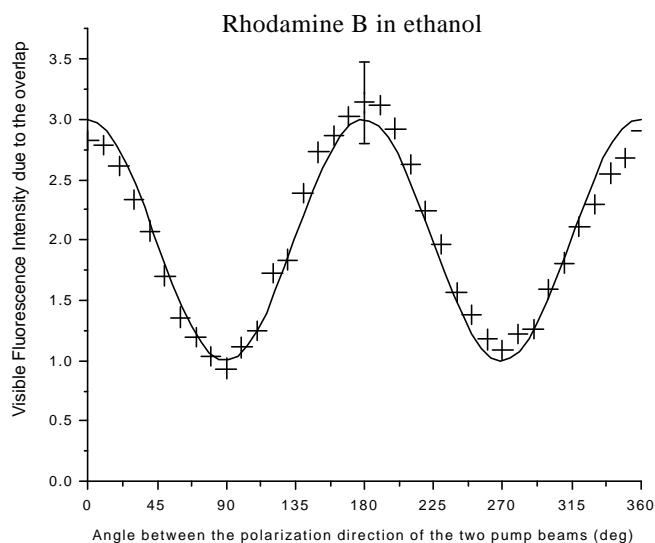
Figure 5. Polarization dependence of visible light emission excited by non degenerate TPA/E in 10^{-3} M rhodamine B in ethanol. The excitation wavelengths were 900 and 1243 nm. 0, 180 and 360 deg. in this plot correspond to parallel polarization. The dashed curve is a $\cos^2(\theta)$ fit to the data with a constant value added since the signal at perpendicular polarization is not zero.

At first glance a dependence of the emitted light on in TPA/E is unexpected. After all, the medium is isotropic, the dye molecules are randomly oriented and the emission process should have no memory of the orientation of the light fields that were absorbed. On second thought, it may be possible that two photon absorption itself is stronger when the beams are polarized parallel to each other. A simple model of the process of two photon absorption due to two intersecting beams is given below. When the two photon interaction is averaged over all possible orientations of the molecules it yeilds a $\cos^2$ dependence is understandable. A dependence of TPA/E on the relative polarizations of the two light beams has been reported previously and a very detailed model proposed [5]. That model and the simpler model below supports the preceding data, giving a ratio of 3 between maximum and minimum two photon absorption. [1]

We now show that the dependence observed thus far can be explained by calculating the dipole induced in a molecule by the interaction of the two fields in the medium. We then find the average value of this induced dipole to account for the many possible orientations of the molecules in the intersection volume. Figure 6 gives the geometry and defines the angles used in the following discussion.
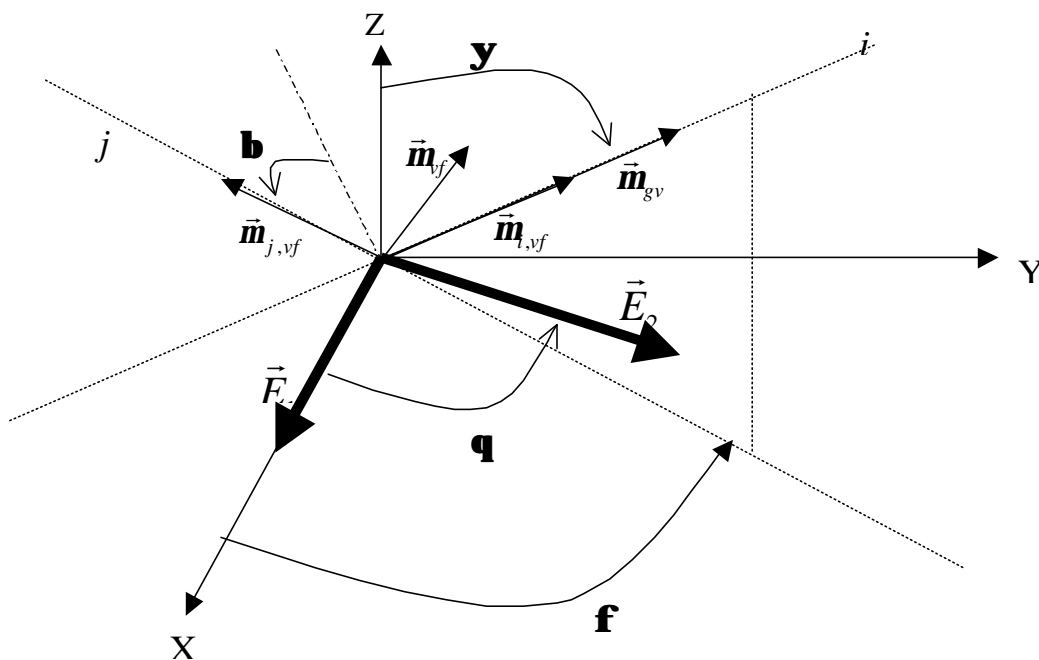
Figure 6. The coordinate system used in developing the model of the polarization dependence of two photon absorption at the intersection of two pump beams.

---

[1] In work conducted near and since the end of the current program as discussed below we have obtained experimental results that can not be explained by either model. We are evaluating that data and working to develop a more complete model.

To understand two-photon absorption due to two intersecting beams we must evaluate the effect of one pump beam on the absorption of the other as they interact in the medium. The fields from the two pump beams interact through the dipole induced in each molecule. To calculate the absorption of the beam at frequency w_1 it is necessary to calculate the polarization at frequency w_1 induced by a combination of the incident fields. This is done by combining the fields at frequencies w_1, w_2 and $-w_2$. The various terms in the induced dipole can be evaluated using a detailed quantum theoretical approach.[1] However, here it suffices to build on such results to provide a simplified explanation of the observed phenomenon. Each term in the sum of quantities giving the induced dipole in a single molecule resulting from the interaction of three incident fields is composed of a product of three dot products of the form $\vec{m}_{mn} \cdot \vec{E}(w)$. In this product, $\vec{m}_{mn}$ is the dipole moment for the transition between states n and m defined by the integral $\int u_m^* e\hat{r} u_n d^3r$. u_m is the spatially varying part of the wave function corresponding to the energy E_m, e is the electric charge and $\hat{r}$ is the position operator. $\vec{m}_{mn}$ is a characteristic of a particular molecule hence all the molecules of a given dye have the same transition dipole moment, $\vec{m}_{mn}$, connecting the states of energy E_m and E_n. In addition, each of the terms in the sum giving the induced dipole moment is divided by the product of three frequency differences that include damping. The damping gives rise to two-photon absorption. Resonances in the two-photon process occur when either incident light frequency or their sum frequency corresponds to a real transition of the molecule.

It is necessary to average the relevant dipole over all possible orientations. First consider the dipole transition moment $\vec{m}_{gv}$ between the ground state g and a virtual state v having energy $\hbar w_1$. This virtual state is not a physical state but a superposition of all the other states available to the electron. As indicated in Fig. 4 let $\vec{E}_1$ lie along the x-axis and ($\vec{E}_1, \vec{E}_2$) define the (x,y) plane. Call i the axis defined by the direction of the dipole moment $\vec{m}_{gv}$. With this choice of system coordinates the dot product of $\vec{m}_{gv}$ with the electric field $\vec{E}_1$ at frequency w_1 is:

$$\vec{m}_{gv} \cdot \vec{E}_1(w_1) = m_{i,gv} \cos j \, \sin y E_1(w_1) \tag{1}$$

Now consider the dipole transition moment $\vec{m}_{vf}$ between the virtual state v and a state f having energy difference $\hbar w_2$ with state v. This dipole transition moment can be written as the sum of two components, one parallel to the dipole moment $\vec{m}_{gv}$ that we call $m_{i,vf}$ and one lying in the plane perpendicular to it, $m_{j,vf}$. The dot product of this dipole transition moment with the electric field $\vec{E}_2$ is:

$$\vec{m}_{vf} \cdot \vec{E}_2(w_2) = \left(m_{i,vf} \cos(j-q) \sin y - m_{j,vf}(\cos b \cos y \cos(j-q) + \sin b \sin(j-q))\right) E_2(w_2) \tag{2}$$

Here, j is the angle between the projection of the axis i into the (x,y) plane and the positive x axis, y is the angle between the z axis and the axis i in the plane of these axes, β is the angle between the normal to the axis i in the plane of the i and z axes, and the direction of the j component of the dipole transition moment $\vec{m}_{vf}$, and θ is the angle between $\vec{E}_1$ and $\vec{E}_2$ in the (x,y) plane.

Since the molecules are randomly oriented, one must average y over 0 to π, j over 0 to 2π, and, since the molecule can be rotated around its own axis by an angle b, one must average b from 0 to 2π. The component of the average polarization in the medium that is parallel to $\vec{E}_1$ is therefore proportional to:

$$\left\langle \vec{P}(w_1) \right\rangle_{\vec{E}_1} \propto \frac{1}{4p^3} \int_0^{2p}\int_0^{p}\int_0^{2p} \left(\vec{m}_{gv}\cdot\vec{E}_1(w_1)\right)\left(\vec{m}_{vf}\cdot\vec{E}_2(w_2)\right)\left(\vec{m}_{vf}\cdot\vec{E}_2^*(w_2)\right)m_{gv}\cos j \, \sin y \, dj \, dy \, db \tag{3}$$

$$\propto E_1 |E_2|^2 \frac{1}{512}\left[2\left(12m_{i,gv}^2\left(2m_{i,vf}^2 - m_{j,vf}^2\right)\right)\cos^2 q + 4m_{i,gv}^2\left(6m_{i,vf}^2 + 13m_{j,vf}^2\right)\right]$$

The coefficient of two-photon absorption is given by the imaginary part of $\dfrac{\left\langle \vec{P}(w_1) \right\rangle_{\vec{E}_1}}{E_1}$ and significant two photon absorption occurs when there is a real state at the energy $\hbar(w_1 + w_2)$. Therefore, the two photon absorption coefficient α_{TPA} of the field at frequency w_1 is:

$$a_{TPA} \propto |E_2|^2 m_{gv}^2 m_{vf}^2\left[\left(6\left(2 - 3\sin^2 g\right)\right)\cos^2 q + \left(6 + 7\sin^2 g\right)\right] \tag{4}$$

In expression 4, m_{gv} and m_{vf} are the dipole moment between the ground state and the virtual state v and between the virtual state v and the final state, respectively, and γ is the angle between the transition dipole moments direction. α_{TPA} is proportional to the intensity of the field at w_2, contains one term proportional to $\cos^2 q$ and a second term that is independent of θ.

Certain special cases of the proportionallity in expression 4 provide insight into the observed phenomenon. When the transition dipole moments are parallel to each other, so that $\gamma = 0$, the two photon absorption coefficient becomes:

$$a_{TPA} \propto |E_2|^2 m_{gv}^2 m_{vf}^2\left[2\cos^2 q + 1\right] \tag{5}$$

which is exactly the functional form for the dependence on θ found experimentally in low viscosity solvents (See Figs. 2 and 3). This clear agreement between the model and experiment allows us to say that in our dye molecules, the two dipole transition moments are parallel to one another.

If $g = 54.7$ deg, there will be no dependence of the two-photon absorption coefficient on the angle θ. When the two transition dipole moments are perpendicular to each other, eg. when $\gamma = 90$ deg, the proportionallity becomes:

$$a_{TPA} \propto |E_2|^2 m_{gv}^2 m_{vf}^2\left[-6\cos^2 q + 13\right] \tag{6}$$

Such a dependence, where the maximum signal occurs when the fields are perpendicular to each other is not observed. This supports the conclusion that the dipole transition moments are parallel to each other in our dye molecules.

In recent months additional data on the polarization dependence has been obtained that demonstrates a dependence of the ratio observed on the viscosity of the solvent as shown in Fig. 7. Further, Fig. 8 shows the one and two photon excitation spectra and the emission spectrum of the dye napthofluorescein in ethylene glycol. The colored pairs of vertical lines along the wavelength scale indication pairs of excitation wavelengths used to excite emission by non degenerate two photon absorption in this dye. In Fig. 9 we show the emission strength versus the angle between the polarizations of the excitation beams for the pairs of excitations wavelengths indicated in Fig. 8. Clearly the ratio depends on the choice of wavelengths and in the case of excitation accessing the strongest two photon excitation band the ratio is 4. Experimental results for rhodamine B shown in Fig. 10 confirm that there is a dependence of the ratio on the transition accessed in the two photon process. These features will be explored further and a model will be developed to explain them in subsequent research.
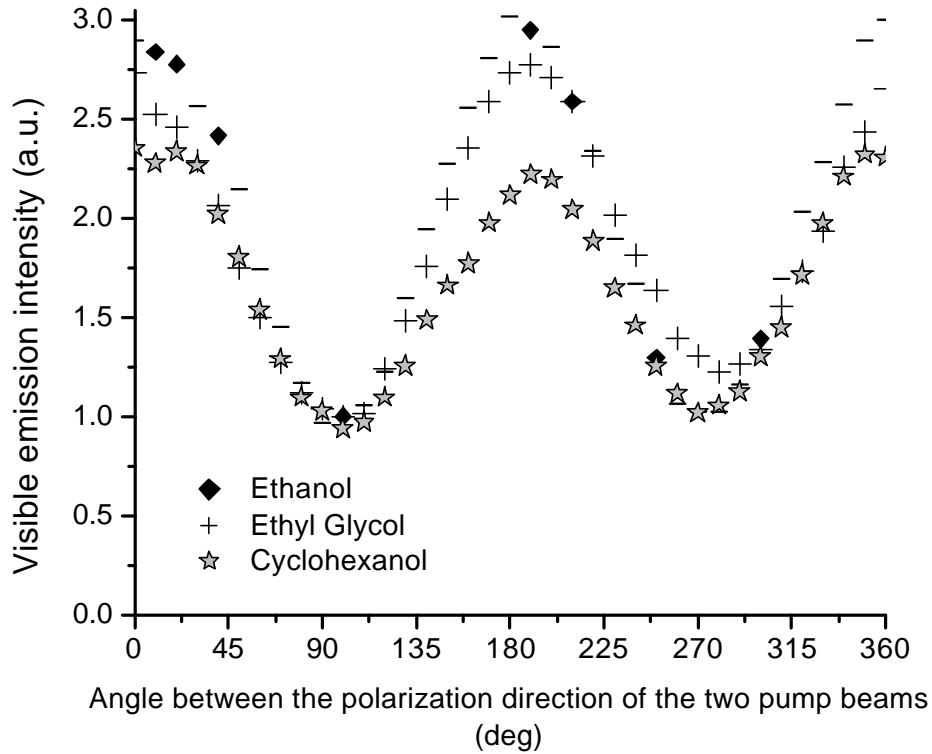
Figure 7. Experimentally observed visible light intensity normalized to one at the minimum versus the angle between the polarizations of the pump beams in the case of non degenerate two photon absorption. The emitting dye is coumarin 7 and the excitation wavelengths are 720 nm and 1074 nm. The squares are the data points measured in ethanol (viscosity 1.1), the crosses are measured in ethyl glycol (viscosity 16.1) and the stars are measured in cyclohexanol (viscosity 57.5).

Naphtofluorescein in Ethylene-Glycol
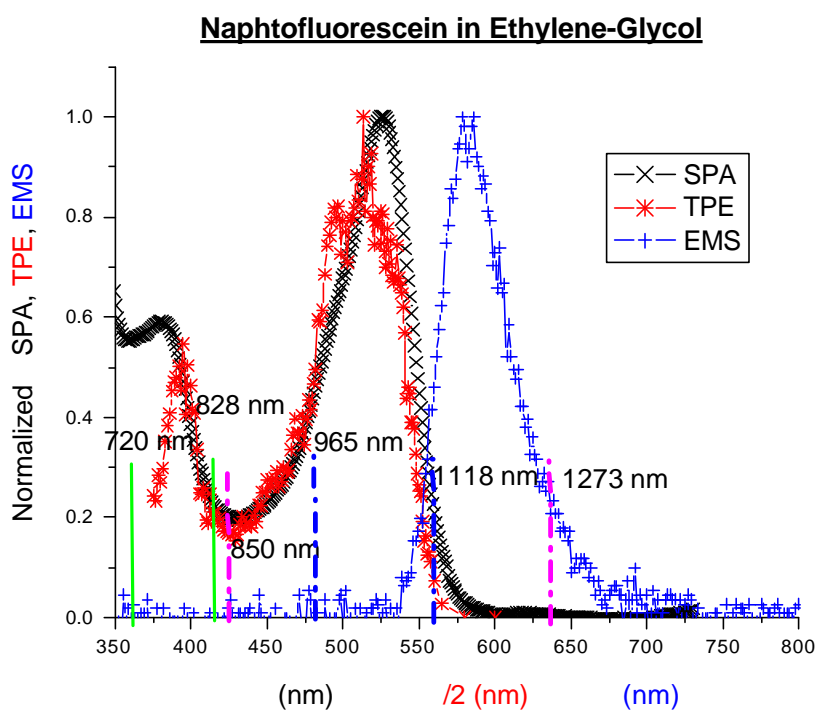
Figure 8. The normalized one and two photon excitation spectra and the emission spectrum of napthofluorescein in ethylene glycol. The pairs of vertical colored lines indicate pairs of wavelengths used in non degenerate two photon excitation experiments and are coordinated with the colors of the data points in Fig. 9.

Data: Data9_E
Model: polaricos2

Chi^2/DoF   = 0.01267
R^2   = 0.99

A   1.000   ±0
K   2.96699   ±0.03379
x0   6.78632   ±0.58923
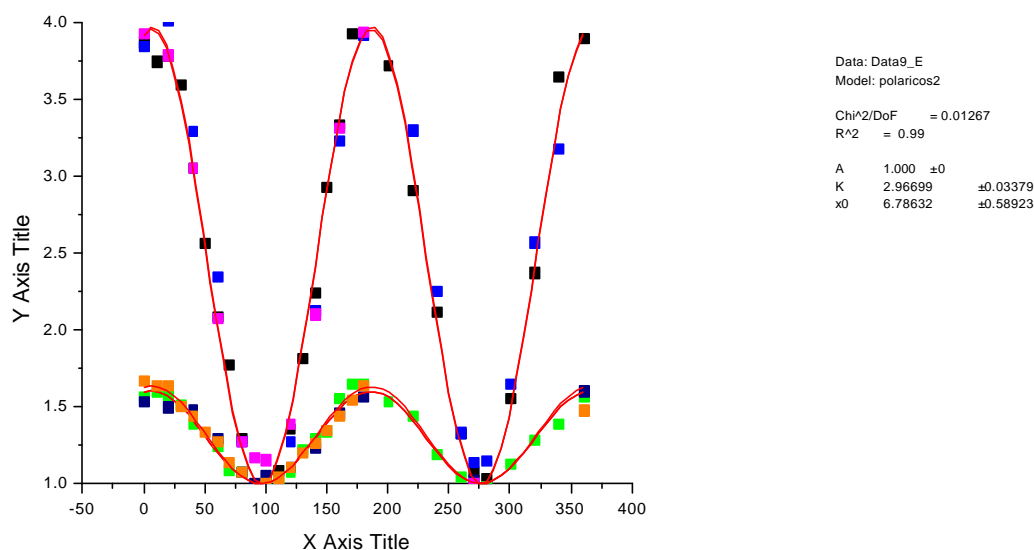
Figure 9. The normalized two photon excited emission strength (Y) versus the angle between the polarizations of the two beams (X) used to induce non degenerate two photon absorption for naphtofluorescein in ethylene glycol.

15
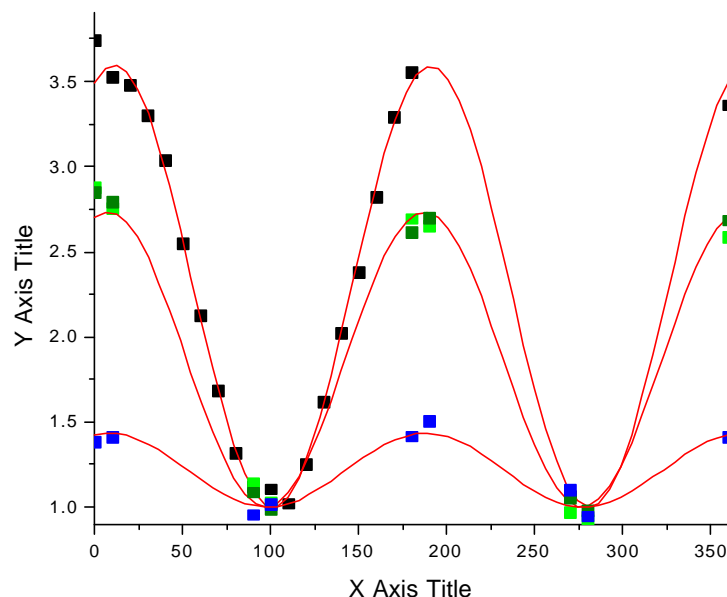
Figure 10. The two photon excited emission strength of rhodamine B in ethylene glycol (Y) versus the angle between the polarizations of the two beams used for excitation (X) for the three different excitation wavelength pairs shown in Fig. 3.

We now comment on the observed effect of the solvent viscosity on the ratio measured between the signal detected when the two pump beams have parallel polarization and when they have perpendicular polarization. Fig. 7 shows the visible emission detected as the angle between the polarization of the two pump beams is rotated between 0 and 360 deg in a solution of Coumarin 7 in ethanol, in ethyl glycol and in cyclohexanol. The ratio of maximum visible signal to minimum visible signal clearly decreases as the viscosity of the solvent increases. The same observation was made when using different dyes in different solvents. We believe that this effect may be related to the geometry of our detection system and as discussed below is a critical feature to be considered in 3D displays using non degenerate two photon excitation. In the high viscosity solvents, the molecules do not have time to randomly orient themselves before they fluoresce (on the order of a few nanoseconds). Therefore when the two pump beams are parallel polarized, the molecules that are most excited are aligned so that their dipoles radiate more strongly in the plane perpendicular to their orientation (see Fig. 4). The signal collected by our detection system sketched in Fig. 4 is low. When the two pump beams are perpendicular polarized, the molecules that are most excited are at some angle with resepect to the direction of propagation into the detection system. Our detector then collects a larger part of the radiation emitted, even though the excitation is smaller. The ratio of maximum to minimum signal detected is then less than maximal.

In a solid, the viscosity is very large. It is therefore very important when designing a 3D display to think through the geometry of the excitation as well as of the detection in order to optimize the output. The excitation is larger when the two pump

beams are linearly polarized parallel to each other, and the visible signal radiated is stronger in the plane perpendicular to this common direction of polarization.

The polarization dependence also applies to other applications of two photon processes such as data storage and two photon photo-polymerization for manufacturing micro-miniaturized devices. In these applications one must take care to design optics that insure parallel polarization for both beams.

In addition to the work in Ref. 2 showing the potential of commercially available dye doped plastics for 3D displays we have worked with colleagues in France on sol gel hosts for dyes for this application.[6] Several combinations were tested, some were of interest and are the subjects of continued study. Others suffered laser induced damage and were discarded. The work in Ref. 3 includes a criterion for voxel visibility that has proven quite useful in evaluating materials. This criterion, obtained by considering the number of photons that will enter the eye at a certain distance from a voxel when the voxel is excited by TPA/E, is given as: $N = \frac{1}{4\pi} \frac{X}{h\bar{\nu}_{ir}} \frac{d_e^2}{L^2} \frac{E_p^2}{\tau_p} \frac{1}{d_v}$. Here N is the number of photons that enter the eye of diameter d_e, at a distance L from a voxel of diameter d_v when excited by two photon absorption of a pulse of energy E_p and duration τ_p and $\bar{\nu}_{ir}$ is the median of the two near infrared frequencies used. X is the two photon absorption coefficient given by the product of the two photon absorption cross section with the density of molecules in the voxel. In the Handbook of Perception and Human Performance we find that the dark adapted human eye can detect about 100 photons in the mid visible. Based on this criterion some of the dye doped systems that we have studied such as coumarin 7 and rhodamine B will produce easily detectable voxels at reasonable viewing distances (eg. ~ 1 m). They will do this while using the amounts of energy modest diode lasers would deposit in the voxel during a dwell time of the light in the voxel (eg. the effective τ_p).

One of the desired features of a 3D display is an ability to display different colors. This means that we must search for dye doped materials that can emit red, green and blue light and then develop means to locate these emitters in each voxel. The choice of excitation wavelengths will allow excitation of different colors. To locate more than one type of emitter in each voxel we prepare the emitting material in the form of particles smaller than the voxel diameter and disperse them in a polymer host (eg. PMMA or a variant thereof) so that there are many of each type in each voxel. This research required careful study of grinding and preparing small particles so that the grinding damage does not adversely affect the TPA/E excited emission. Initial work on preparing particles of crystalline materials has shown how difficult this can be. In addition, the dye doped material is physically soft and therefore difficult to grind.

The idea of using dispersed particles of materials that can emit visible light by TPA/E allowed us to re-visit the issue of using crystalline up converters for 3D display applications. While many doped crystals have been shown to be good up converters they

can not be scaled in size to make a practical 3D display. We have studied the use of powders of such crystals that can be excited by TPA/E to emit visible light in 3D displays. We identified from our own and others prior work crystals with promise. [7] One important feature of up conversion in doped crystals is that there exists the possibility of sequential two photon absorption. This process involves sequential absorption of two photons by transitions between real states and is, therefore, more efficient than the simultaneous process in the dyes discussed above. Using our dual parametric oscillator pump source we started to evaluate rare earth doped fluorides crystals for sequential up conversion. When the preferred excitation wavelengths are determined we will prepare powders of the most promising and disperse the powders in an appropriate passive host medium. Such a passive host will, ideally, have the same index of refraction as the particles dispersed in it so as to minimize scattering. We plan to test these dispersed crystallite media for 3D display demonstrations.

Preparing powdered crystals while preserving their spectroscopic properties requires careful grinding and post grinding treatments. In the grinding process a great deal of subsurface and surface mechanical damage was done to the crystals. Such damage provides quenching sites for fluorescence. The damage also makes color center formation easier providing yet another quenching mechanism. Further, impurities can enter through surface damage and affect the material's spectroscopic properties. The powders we prepare are examined microscopically to identify surface damage due to grinding. We have started to study post grinding annealing or etching of the crystalline particles to remove grinding damage. These steps are also necessary if the particles are to be dispersed in a passive host and the resultant medium is to be optically clear and scatter free. We have already made progress towards this goal as describe below in the discussion of optically written 2D displays. That is, we have developed a form of phosphorylated-PMMA that can contain crystalline particles without cracking and we have learned the use of surfactants to more uniformly disperse the crystallites.

Optically Written 2D Displays:

We have demonstrated a concept for 2D information display that uses laser diodes emitting at 970 nm to excite visible emission from up-converter materials[2, 3]. The light from these diodes is scanned onto a screen that is covered with a material, which efficiently up-converts the infrared photons into blue, red or green light. as sketched in Fig. 11. Fig. 11 shows that our concept is obviously similar to an electron beam written CRT display. The advantages offered by such a system are several. To list a few, it can easily be scaled from small to large sizes (by using several diodes and tiling if necessary) without the depth problems inherent to the CRTs (the optical path can easily be folded). The new system does not require a heavy vacuum tube or high voltages which makes it safer (the laser radiation is filtered and never gets out of the apparatus). The infrared photons used have low energy so they do not damage the screen material. The display lifetime should be limited by the diode laser lifetime ($\sim 10^4$ hrs), and this could be replaced easily when necessary. The brightness obtained depends directly on the pump intensity and is limited by saturation only for very high pump exposure. With proper understanding and engineering, it should be possible to make a display of very high luminance. We therefore have demonstrated red, green and blue emitters and studied the

physics of the up-conversion process to enable design of a system with optimized properties.

Up-conversion materials have been known and studied for decades as possible laser materials. We started this study by looking at fluorides crystals doped with several rare earth ions which had been shown to be efficient up-converters in the past[4, 5, 6]. Because these crystals can not be prepared in sizes as large as needed for most display applications, we prepare the crystals as ~10 μm size particles and disperse them in a phosphorylated polymethylmethacrylate (p-PMMA) host. We had to develop this host since ordinary PMMA could not stand the internal stresses of forming around the crystalline particles. In developing this host we worked with Prof. K. Belfield of the UCF Chemistry Department and have submitted a patent disclosure on this concept. The p-PMMA with crystalline particles results in a display medium that can be formed to any desired shape, can be transparent or not, as desired, and can be affixed to any desired substrate.
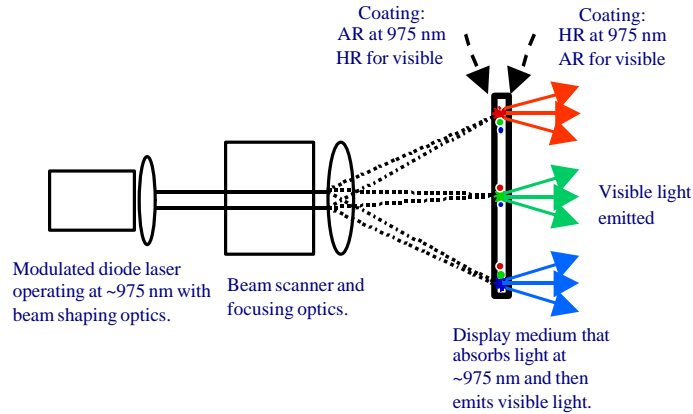

Figure 11. Schematic diagram of the new 2D display concept.

Experiments have been conducted using several different rare earth ions co-doped with Yb^{3+} in fluoride crystalline hosts. Unlike crystalline materials for 3D displays the Yb^{3+} co-doped materials are excited by a single wavelength of light. That is, the Yb^{3+} ions absorb light in a fairly broad band near 975 nm in these crystals and then efficiently transfer the absorbed energy to levels of the co-dopant from which visible light can be emitted. While this type of crystal would not be useful for a 3D display, it could have implications for an optically written 2D display. The excitation process, one in which sequential absorption of two photons of near infrared energy by donor ions which then transfer that energy to a single acceptor ion in a manner that the acceptor can then emit visible light, is a form of sequential up-conversion. Table I is a list of the various crystals and co-dopants that we have studied so far and the central wavelengths of the bands of visible emission detected following excitation with a diode laser source operating at 968 nm. Fig. 12a shows the emission spectrum obtained from $Yb:NaYF_4$ co doped with Tm^{3+} ions, 12b with Ho^{3+} ions and 12c with Er^{3+} ions. We note that the emission lines are

fairly narrow (characteristic of rare earth ions) so we can obtain strong saturation of colors by mixing the blue, green, and red.

Table I: Visible emission wavelength of Tm, Er and Ho after Yb excitation in different fluoride hosts

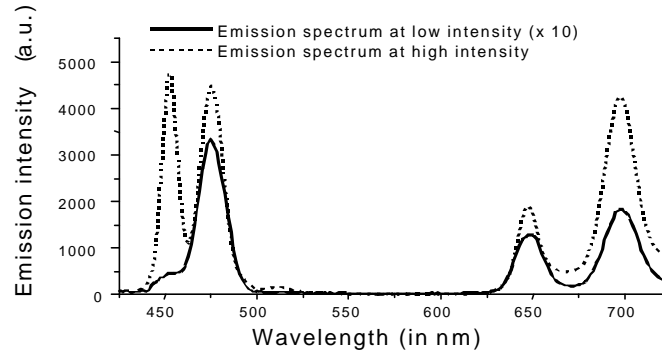| Doping ion Yb^{3+} +	Crystal host	Peak emission wavelength (nm)		
		blue	green	Red
Tm^{3+}	NaYF$_4$	450, 475		647, 698
	KYF	481		652
	YLF	483		648
Er^{3+}	NaYF$_4$	411	540	660
	KYF		550	654, 670
	YLF		541, 549	654, 668
Ho^{3+}	NaYF$_4$		540	648
	KYF		544	658

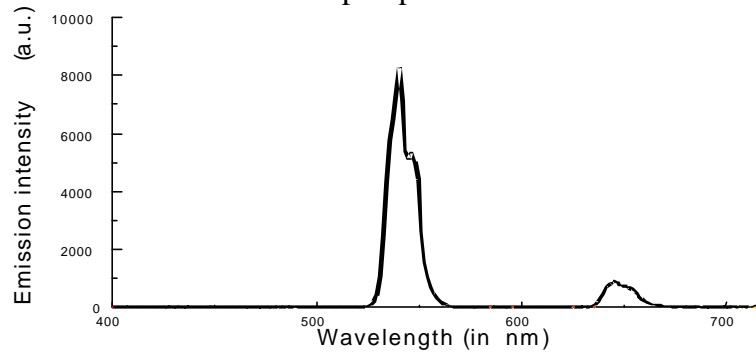Figure 12a. Emission spectrum of Tm,Yb:NYF after excitation at 968 nm and for different pump intensities

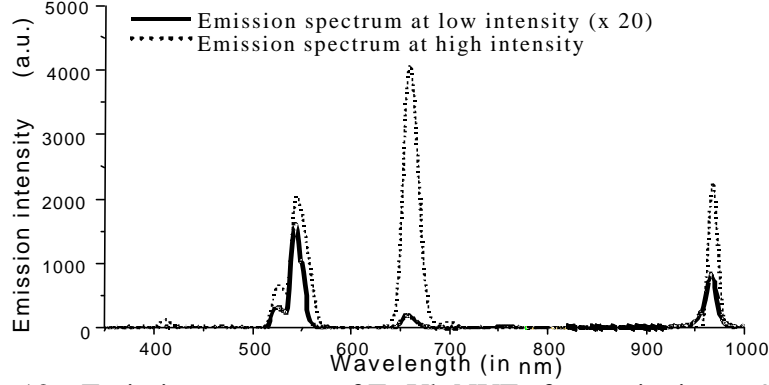Figure 12b. Emission spectrum of Ho,Yb:NYF after excitation at 968 nm

Figure 12c. Emission spectrum of Er,Yb:NYF after excitation at 968 nm and for different pump intensities

As seen from the emission spectra, the relative strength of emission at different wavelengths depends on the pump intensity. Furthermore, because the process of visible emission implies absorption of more than one infrared photon, at a given wavelength the emission strength does not vary linearly with the pump power. It is critical to understand the role of each parameter involved in the excitation and emission process in order to optimize the efficiency of an optically written up conversion display. Therefore, we developed a simple model of up-conversion that allows us to predict and to scale such displays.

The energy diagram associated with our coupled system of ions (ytterbium plus visible emitter) is described in Fig. 13 for the case of Yb-Ho. Because the proper parameters are not yet available for our more efficient materials, we used values found in the literature[7] for this particular material. The numerical values used in Ref. [9] were measured for a material designed to make a 2.9 µm laser . The quantitative values obtained for efficiencies should therefore be ignored. We are only interested in the qualitative behaviors of the visible emission for various operating conditions. These behaviors lead us to experimentally confirmed rules for the functioning of our displays.

In order to better understand the mechanism of up-conversion, we first looked at the green visible emission after energy transfer from only two excited Yb^{3+} ions as described in Fig. 13. The rate equations describing the dynamics of the coupled system of ions were written in Mathcad and were:

$$
\begin{cases}
\dot{n}_1 = -\dfrac{\sigma_{abs}I_{pump}}{h\nu}\left(n_1 - n_2\right) + \dfrac{n_2}{\tau_2} + \chi_1\, n_2 n_3 + \chi_2\, n_2 n_4 \\[2ex]
\dot{n}_2 = \dfrac{\sigma_{abs}I_{pump}}{h\nu}\left(n_1 - n_2\right) - \dfrac{n_2}{\tau_2} - \chi_1\, n_2 n_3 - \chi_2\, n_2 n_4 \\[2ex]
\dot{n}_3 = -\chi_1\, n_2 n_3 + \dfrac{n_4}{\tau_4} + \dfrac{n_5}{\tau_5} \\[2ex]
\dot{n}_4 = \chi_1\, n_2 n_3 - \dfrac{n_4}{\tau_4} - \chi_2\, n_2 n_4 \\[2ex]
\dot{n}_5 = \chi_2\, n_2 n_4 - \dfrac{n_5}{\tau_5} \\[2ex]
\dot{\phi} = A_{53} n_5
\end{cases}
\tag{7}
$$

In these equations, n_i represents the population density in the state i, σ_{abs} is the absorption cross-section of the material at the pump wavelength, I_{pump} is the pump intensity, h is Planck constant and ν is the pump frequency. $\dot{\phi}$ is the photon emission rate in the visible and A_{53} is the radiative decay rate of the transition 5 to 3. The system of equations was solved for various initial conditions and the numerical parameters used in the rate equations are listed in Table 2. In order to simplify further the problem, back transfer from the emitter to Yb was ignored in the model.

We first solved the rate equations were solved in the case of equilibrium corresponding to a pump laser beam that does not scan the display but simply stands still on one point. As a result, we obtain a point source of visible light excited by a near infrared diode laser. The calculated power of visible light emitted per unit volume of material (directly related to brightness) versus the pump intensity is shown in a log-log plot in Fig. 14. At low pump intensity the emission varies as the square of the pump intensity. Then there is a significant pump intensity range in which the variation is linear. Finally, for very high pump intensities saturation sets in when the Yb population is nearly equal in both its states.
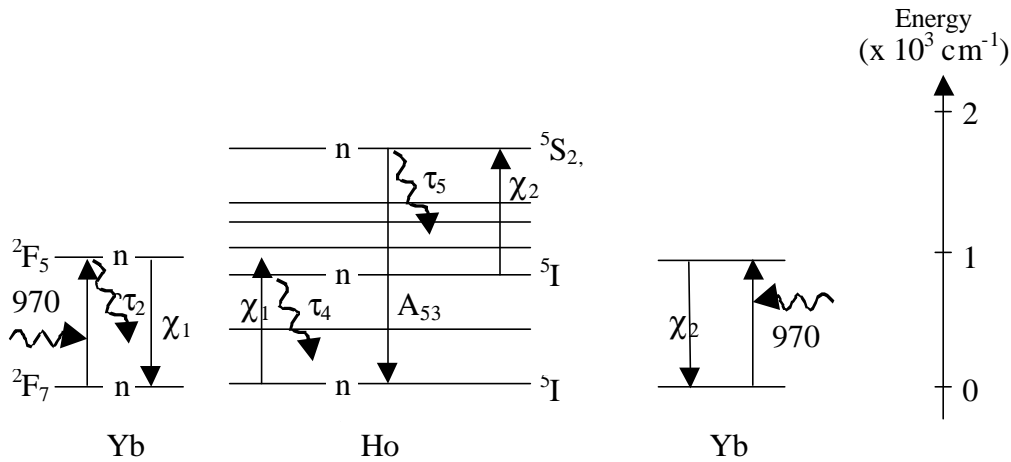

Figure 13. Simplified energy diagram of the coupled system of ions considered.

Table 2: Parameters used in the system of rate equations

Lifetimes	Yb excited state	τ_2	1.8 ms
	Ho intermediate $^5I_6$ state	τ_4	3.5 ms
	Ho upper $^5S_2, ^5F_4$ state	τ_5	190 µs
Energy transfer coefficients	$^2F_{5/2} \quad ^2F_{7/2}$ while $^5I_8 \quad ^5I_6$	χ_1	7 x 10^{-18} cm^3/s
	$^2F_{5/2} \quad ^2F_{7/2}$ while $^5I_6 \quad ^5S_2, ^5F_4$	χ_2	3.1 x 10^{-8} cm^3/s
Radiative decay rate	$^5S_2, ^5F_4 \quad ^5I_8$ transition	A_{53}	3982 s^{-1}
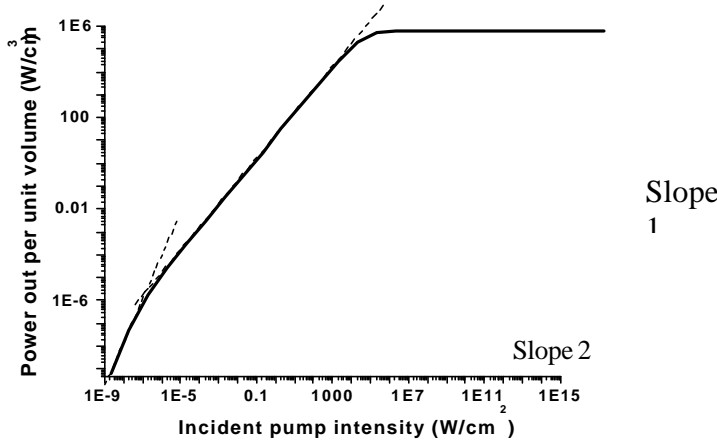
Figure 14. Power of visible light emitted versus infrared pump intensity. Results of simulation.

It is possible to calculate the efficiency of the system used in our model development as defined by the ratio of the number of photons emitted to the number of pump photons absorbed per second per unit volume. As expected, Fig. 15 shows that efficiency increases linearly at low intensity, reaching a maximum value when the emission is linear as a function of the pump intensity. Saturation is not evident in Fig. 15 since when the Yb population is equal in both levels, it does no longer absorbs pump light. The rate with which pump photons are absorbed remains constant when the incident intensity is increased and so the efficiency remains constant.

Figure 15. Emission efficiency versus infrared pump intensity. Results of simulation.

These results were tested experimentally for a sample of Yb, Er:NYF which also emits in the green after energy transfer from two Yb ions. The quadratic and 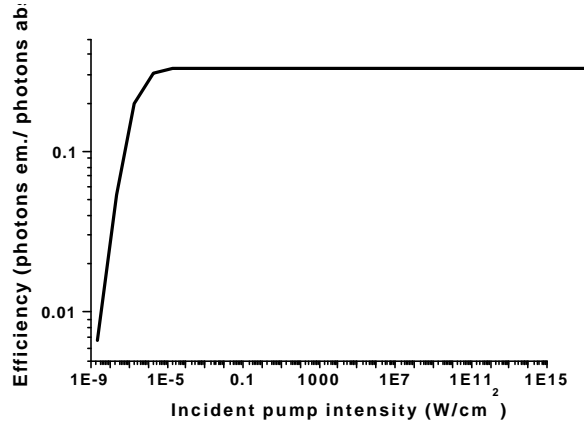linear regimes were observed and are plotted in Fig. 16. We never attained saturation even for brightnesses greater than 50 kCd/m^2. The agreement with the model gives us confidence in saying that we can increase the efficiency of our materials by simply focusing the pump light to smaller spots until we reach a given value of luminance (fixed by parameters intrinsic to the material). The efficiency will then remain constant whether the focus spot is reduced further or the pump power is increased.

We can formalize the expressions for brightness and efficiency in the quadratic regime of the material when the pump beam stands still. The brightness and the infrared pump power P and diameter d are related as follows:

$$B \propto \frac{P^2}{d^4} \tag{8}$$

The efficiency can be written as:

$$\text{Efficiency} \propto \frac{P}{d^2} \tag{9}$$
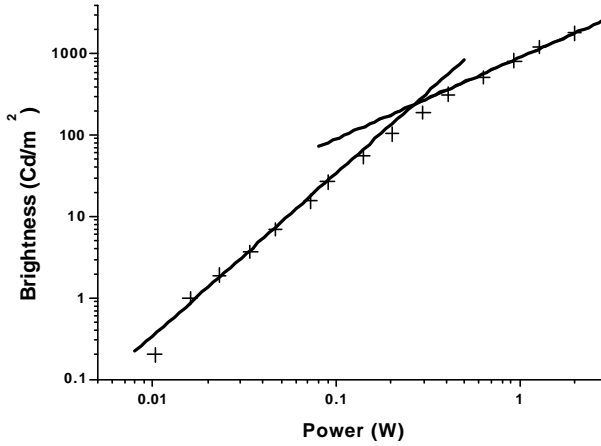
Figure 16. Brightness at 545 nm measured for a sample of Er,Yb:NYF versus incident 968 nm pump power.

The system of rate equations was then solved after excitation by a pump pulse having the following time dependence between t=0 and t=T:

$$I = I_0 \left(\cos\left(\frac{2\pi t}{T} + \pi \right) + 1 \right) \tag{10}$$

This approximates the case in which the pump beam is scanned over a screen with a dwell time of T on each point. The energy emitted per unit volume was calculated for different pulse lengths T but constant pump exposures (product of pump intensity I_0 by pump length T). The result of the calculations is shown in Fig. 17. Several observations can be made from this plot. First, for pump pulse lengths smaller than the Yb excited state lifetime, the emitted light energy depends only on the total exposure even for very short pulses. This is due to the fact that Yb ions absorb the pump photons at a rate

proportional to the pump intensity, then in effect store this energy while transferring to the emitters. Likewise, the decrease in output energy for longer pulse lengths at low exposure is due to loss of stored energy through decay of the Yb excited state population. For the highest pump exposure (100 J/cm^2), we observe a decrease of output energy for the shorter pulses. This corresponds to higher pump intensities where saturation is reached and when the populations in both states of Yb become equal.
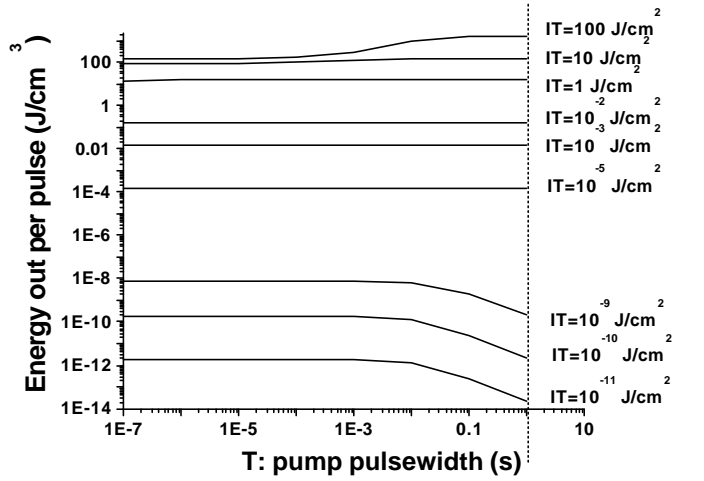
Figure 17.: Energy of visible light emitted per unit volume versus pump pulse length for various pump exposures.

We can also plot these results for a fixed pump pulse length and vary the incident intensities (Fig. 18). As in the static case, three regimes have been observed: quadratic, linear and saturation. It is interesting to note that the transitions between the different regimes occurs for a fixed brightness level, not fixed pump intensity.
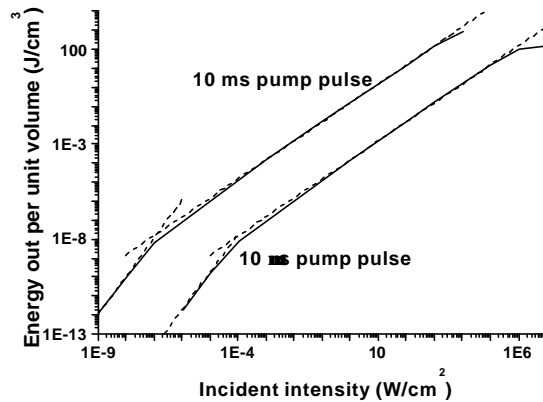

Figure 18. Energy of visible light emitted per unit volume versus incident pump intensity for 2 pulse lengths.

Similarly, we calculate the efficiency as defined by the ratio of the number of photons emitted per pulse and per unit volume of material divided by the number of

pump photons absorbed per pulse and per unit volume of material. The efficiencies for two different dwell times are plotted in Fig. 19 along with the efficiency obtained in the static case. We see from this plot that increasing the pump intensity yields better efficiencies until it reaches its maximum. This maximum occurs at higher intensities for shorter pump dwell times.
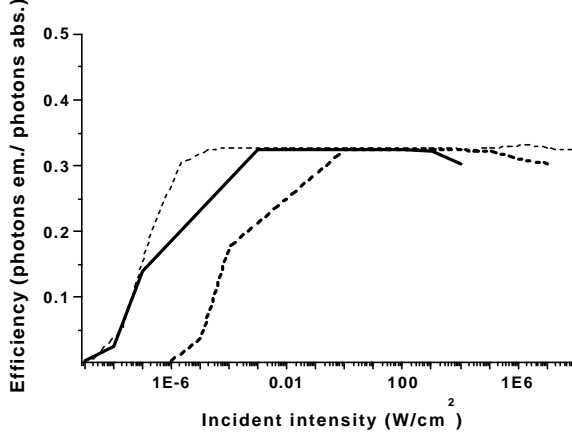

Figure 19. Emission efficiency versus infrared pump intensity for 10 ms dwell time (solid bold curve), 10 μs dwell time (dashed bold curve) and static case (thin dashed curve).

Experiments conducted on a Yb, Er:NYF sample showed that the brightness of the green emission was indeed a quadratic function of the incident beam intensity in the range of intensities available at this time. This gives us confidence for deriving scaling laws for the case of a scanned laser pump beam in the quadratic regime. Assuming a single diode laser of output power P focussed to a spot of diameter d, used to scan a total length L with a repetition rate RepRate, we find that the brightness, B, is

$$B \propto \left(\frac{P}{d^2} \frac{d}{L \ RepRate} \right)^2 RepRate = \frac{P^2}{d^2 L^2 \ RepRate} \tag{11}$$

The corresponding efficiency is:

$$Efficiency \propto \frac{P}{dL \ RepRate} \tag{12}$$

Once again, for the brightness levels desired in a display, we will be working in the quadratic regime of our material. We can therefore predict that the efficiency can be increased by focussing the pump beam to a smaller spot. It can be noted that this study concerns processes in which two energy transfers from Yb are involved. The effect of the pump intensity (power and diameter) on the blue emission from other dopant ions should be even stronger, as the process involves three energy transfers from Yb ions.

We have modeled the effects of the pump intensity and duration on the visible light output and the up-conversion efficiency for optically written 2D displays. The predictions of the model were observed experimentally. The up conversion efficiency depends on the pump intensity and knowing the relationship allows us to design improved pumping schemes for optically written 2D displays. Using the scaling law, with the material and focusing geometry currently studied, we can obtain a display of

30 cm x 30 cm with a brightness of 250 Cd/m^2 and a resolution of 1000 x 1000 using 210 W of laser diode power. This corresponds to about 1.3 lm/W . The scaling rules also show that this result could be improved by taking a few additional steps (e.g., coatings, use of proper pump wavelength). These steps along with proper pixel design will allow such a display to be operated with only 15 W of pump power.[2]

This area of our research, optically written 2D displays, has received significant interest from industry. We are in discussion with Philips Co. to commerciallize this type of display. We are working with a company whose interest arose from our display work but wants to use our concepts for making counterfiet proof marks for products. NEOS Optical Systems has taken an interest in using our optically written 2D display technique to improve their 3D display based on displaying laser light on a rotating spiral. We have shown them that they can convert their display's optics and lasers to one laser at 975 nm and near infrared optics while coating their rotating spiral with our display medium. They will then have a much brighter (eg. more visible in a lit room) 3D display. NEOS has donated a 2D acousto optic scanner to us to further our work. In addition, several patents[8] are being processed to provide intellectual property protection for these university-industry collaborations.

Modulators for 3D displays
A no moving parts, wide angular scan range, large diameter aperture optical beam scanner with ultrafast nanosecond scan setting speeds is a desired module for 3-D displays. Various designs for optical scanners have been proposed including the ones that rely on the use of one or more moving optical components such as mirrors and polygons in combination with electronically controlled inertialess optical devices. These scanner technologies have limited performance and thus fail to satisfy the stringent requirements of the desired 3-D scanner. For instance, acousto-optics has speed but is power hungry (> 1 W), with limited angular beam scan range. Bulk electro-optics requires high voltages whereas integrated electro-optic beam steerers have small aperture sizes with high driving voltage requirements. Recently, optical microelectromechanical systems (MEMS) using micromirrors offer promise, but are presently limited to small apertures (< 2 mm) with a speed versus mirror size dilemma due to the inherent mechanical inertia of these mirror components. Similarly, the use of microlens array to form a scanner is again limited in speed due to the mechanical nature of the beam scanning method.

A novel design technology called Multiplexed Optical Scanner Technology (MOST) was introduced for agile beam steering that promises low power consumption and true rapid three dimensional (3-D) beam forming to accurately control beam position, power and shape. The free-space Wavelength Multiplexed Optical Scanner (W-MOS) is a peer member of the MOST family and has been the focus of our first stage study for 3-D scanners for displays. The scanner gets its power from high-speed wavelength selection coupled with light interaction with a wavelength dispersive element that in turn

---

[2] In work since the end of the reporting period we have demonstrated that the efficiencies of the red, green and blue emitters are in the range of several per cent of the incident power when using the proper pump wavelength and waveform. According to colleagues at Philips Inc. these efficiencies make our optically written 2 D display potentially viable for commercialization.

leads to spatially dispersed beam scanning. This scanner has the potential to scan at gigahertz rates using present-day state-of-the-art nanosecond tuning speed lasers. The free-space W-MOS with its large aperture offers high scanning resolution, e.g., $< 0.01^{o}$ that meets the stringent requirement for wide angle display systems. In this section we briefly discuss two versions of the free-space W-MOS design and describe its power to deliver wide angular scan range and high resolution, all at nanosecond scan setting speeds. The complete theory for the W-MOS has been described in Ref. 2. The experimental results are in complete agreement with the theory and attest to the simplicity and functionality of our proposed novel scanning ultra high speed optical beam scanner.

   Fig.20 shows the two versions of the basic structure of the free-space W-MOS. Fig. 20 (a) shows the design where the wavelength selection is achieved by tuning a laser while Fig. 20 (b) shows the design where beam scanning is achieved by selection of wavelength via a tunable optical filter such as an acousto-optic tunable filter (AOTF) coupled to a broadband source. In both cases, very high speed beam scanning can be achieved using electronically tuned solid state lasers and filters with sub-microsecond response time. Light from the tunable source is collimated, expanded to attain high resolution from the free-space W-MOS design, and strikes a wavelength dispersive element such as a one- dimensional (1-D) grating. The spherical lenses can be chosen and
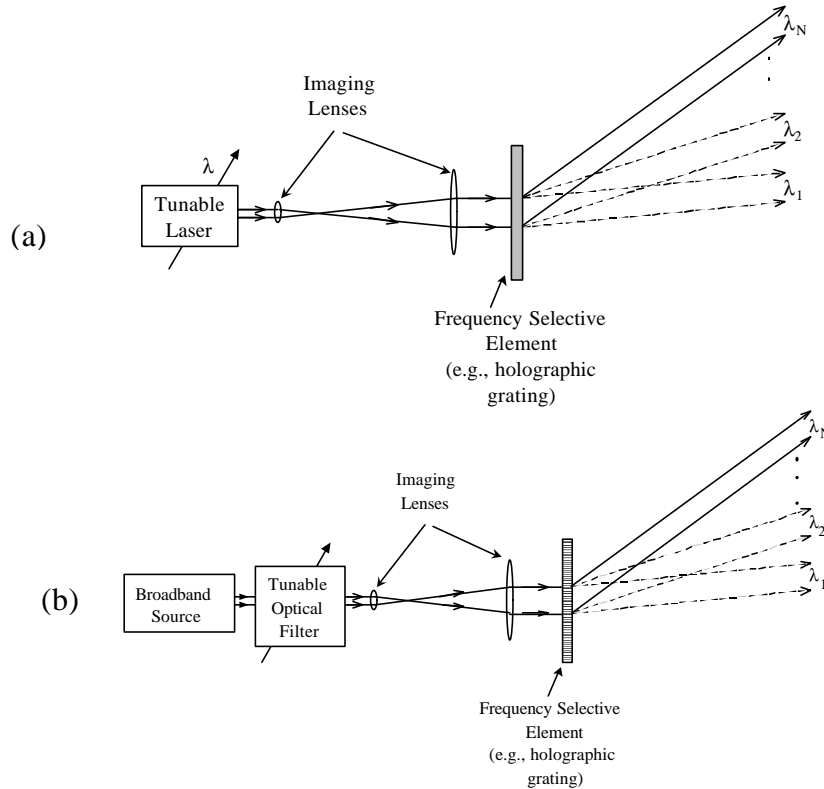

Figure 20. Schematics of free-space version of W-MOS for implementing no moving parts, wide angular scan, ultrahigh speed one dimensional (1-D) optical scanner using (a) a tunable laser and (b) a tunable optical filter cascaded with a broadband source.

adjusted such the minimum beam waist of the collimated light is at the grating for maximum diffraction efficiency. If the incident collimated beam hits the grating at an angle $\boldsymbol{q}_{nc}$, the mth order deflected beam is in the direction $\boldsymbol{q}(m)$ given by

$$\boldsymbol{q}(m) = \sin^{-1}\left\{\frac{m\boldsymbol{l}}{L} + \sin\boldsymbol{q}_i\right\},$$

(1)

where $\boldsymbol{l}$ is the wavelength of the beam and L is the period of the grating. By changing the wavelength via electronic control of the tunable source, the light output from the scanner moves spatially along a defined axis, creating an array of optical dots in space. The period L of the grating can be chosen such that there is only one dispersive order as it would be the desired case in an optimized free-space W-MOS.

A proof-of-concept W-MOS system using a 1-D blazed reflection grating (grating period L = 1/600 mm) as a dispersive element was setup in the laboratory using a fiber-coupled mechanically tuned laser with a 80 nm tunable bandwidth centered at 1560 nm, as shown in Fig. 21 (a). Light from the fiber is collimated by a gradient index (GRIN) rod lens and strikes the 1-D reflection grating mounted on a rotational stage to control the angle of incidence $\boldsymbol{q}_{nc}$. An infrared (IR) camera is used to observe the scanning +1 diffraction order when the wavelength of the tunable laser is changed. The angular deflection is measured by tracking the scanning +1 diffraction order with the help of an iris mounted on a C-channel with one end attached to a rotational stage having the same axis of rotation as that for the reflection grating. The grating was tilted slightly so as to adjust the incidence angle to 2.2^{o}. A total angular scan of 14.75^{o} was measured by the tuning the wavelength of the source from 1520 nm to 1600 nm. Fig. 21 (b) shows that the measured scan angle is in complete agreement with the theoretical angular scan given by Eq. (1). These results attest to the simplicity and functionality of our proposed novel scanning ultrahigh speed optical beam scanner.

We have successfully designed and demonstrated a novel wide angular scan range, large diameter aperture optical beam scanner for ultrafast nanosecond scan setting speeds. The free-space W-MOS offers powerful scanner features in a compact and simple to build and control package leading to potentially wide spread use of this technology for 3-D displays. The present 1-D scan W-MOS can be used for form 2-D raster scanned and 3-D scanners as shown in Fig.22.
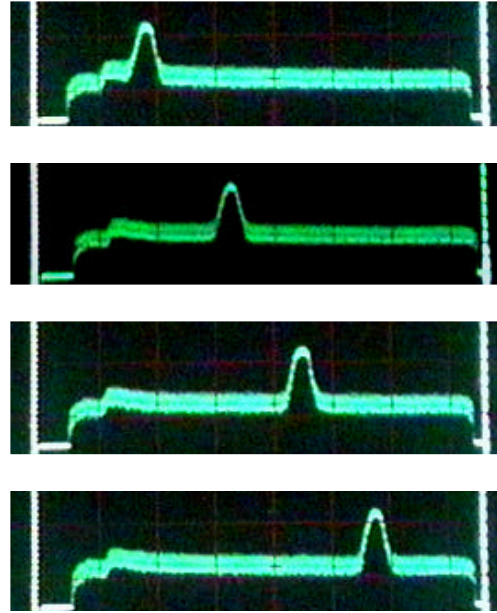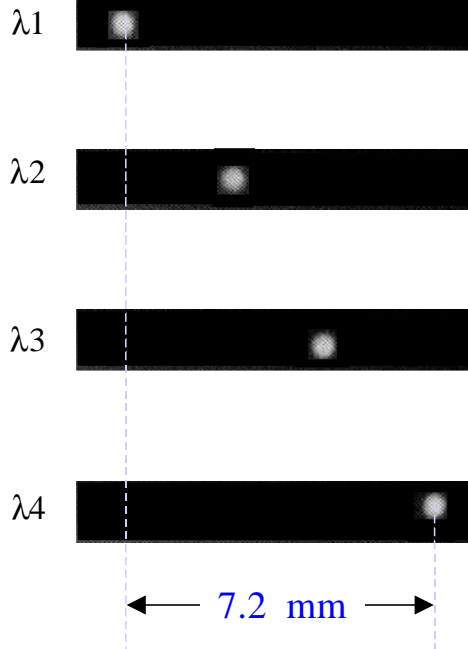
(a)

(b)

Settings

λ1

λ2

λ3

λ4

← 7.2 mm →
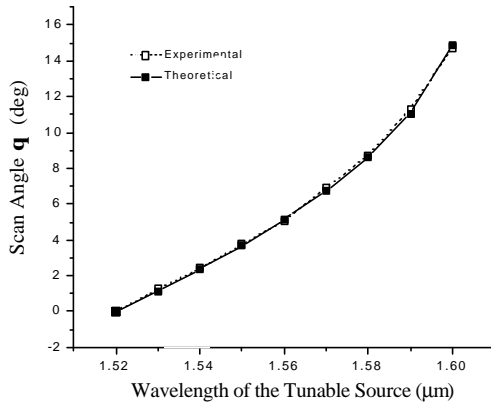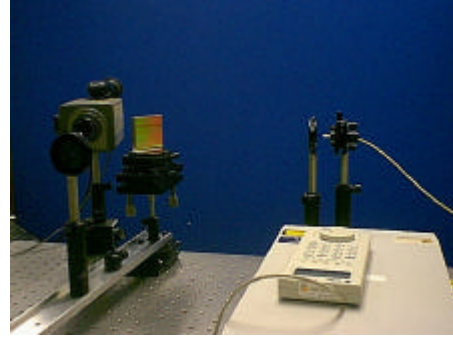
(c)

Fig 21 (a) Theoretical and experimental plots for the scan angle q versus the wavelength of the tunable source, measured for our free-space W-MOS laboratory setup. (b) Our laboratory experimental setup to validate the theoretical angular scan range numbers. 1: Tunable Laser; 2: Optical Fiber; 3: GRIN Lens; 4: Independent Rotational Stages; 5: Blazed Reflection Grating; 6: Infrared Camera; 7: Iris; 8: C-Channel. (c) Infrared camera showing one dimensional (1-D) scanning of spots and their corresponding oscilloscope traces for beam position and beam quality.
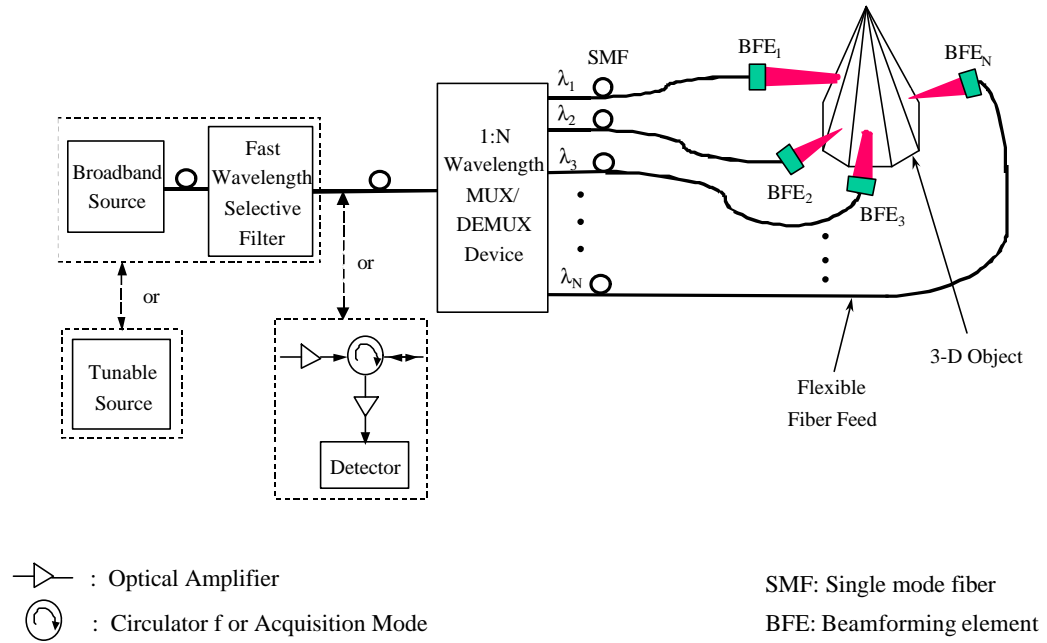
: Optical Amplifier   SMF: Single mode fiber

: Circulator f or Acquisition Mode   BFE: Beamforming element

Fig.22 W-MOS forming a 3-D scanner for use in 3-D displays for 3-D excitation of materials.

LISTING OF PUBLICATIONS AND REPORTS

(a) Papers published in peer reviewed journals
"Dye doped sol-gel materials for two-photon absorption induced fluorescences"
(M. Canva, G.; Roger, F. Cassagne, Y. Levy, A. Brun, F. Chaput, J. P. Boilot, A.
Rapaport, C. Heerdt and M. Bass), Journal of Optical Materials, (2001)

(b) Papers published in non-peer reviewed journals or in peer reviewed conference
proceedings
1. A. Rapaport, F. Szipocs, J. Milliez, H. Jenssen, M. Bass, K. Schafer, K. Belfield,
"Optically written displays based on up-conversion of near infrared light" 20th
International Display Research Conference (SID), Sept. 25-28, 2000 in Palm Beach,
Florida, USA. Paper 4.6.
2. A. Rapaport, F. Szipocs, J. Milliez, H. Jenssen, M. Bass, K. Schafer, K. Belfield,
"Optically written displays based on up-conversion of near infrared light", 7th
International Display Workshops (IDW'00), Nov. 29- Dec. 1, 2000, Kobe, Japan. PH1-3.
3. A. Rapaport, F. Szipocs, J. Milliez, H. Jenssen, M. Bass, K. Schafer, K. Belfield,
"Models of optically written displays based on up-conversion of near infrared light",
Photonics West, Electronic Imaging 2001, Jan. 20-26, 2001 in San Jose, California, USA.
4294-05.

(c) Papers presented at meetings, but not published in conference proceedings
1. A. Rapaport, F. Szipocs and M. Bass, "Dependence of two-photon excitation on the
relative polarization of intersecting pump beams in a dye solution.", IQEC 2002, Long
Beach, CA (May 2002)

(d) Manuscripts submitted, but not published

(e) Technical reports submitted to ARO under grant number: DAAD199910220
1. Interim Report No. 1, Dec. 1999, UCF Report No. 1, UCF Contract No. 65-04-550
2. Interim Report No. 2, March 2001, UCF Report No. 2, UCF Contract No. 65-04-550
3. Interim Report No. 3, March 2002, UCF Report No. 3, UCF Contract No. 65-04-550

LIST OF ALL PARTICIPATING SCIENTIFIC PERSONNEL

Michael Bass, Professor, School of Optics, Principal Investigator
Nabeel Riza, Associate Professor, School of Optics, Co-Principal Investigator
Hans Jenssen, Professor, School of Optics
Kevin Belfield, Professor, Chemistry
Alexandra Rapaport, Post Doctoral Scientist, School of Optics
Janet Milliez, Graduate Student, School of Optics
Ferenc Szipocs, Graduate Student, School of Optics
Katie Schafer, Graduate Student, Chemistry
Alfred Ducharnme, Assistant Professor, Engineering
Jason Eichenholz, Contributing Engineer, Photonic Displays
Arlette Casanho, Owner, AC Materials

REPORT OF INVENTIONS

"Display media using passive hosts in which visible light
emitting particulates excited by two photon absorption of
one or two different frequency optical pump sources are
dispersed"
(M. Bass and H. Jennsen)
U.S. Patent No. 6,327,074

Submitted 10/2/98
Provisional app. 10/22/98

Full application 11/24/99
Claims allowed 9/01
Issued 12/4/2001

"Stabilized Luminescent Polymer Composition"
(M. Bass and K. Belfield)

Submitted 8/2/2000
Accepted as CIP to "DisplayMedia…"

"Display media using passive hosts in which visible light
emitting particulates excited by two photon absorption of one
or two different frequency optical pump sources are dispersed"
(M. Bass and H. Jennsen)

Submitted 12/15/00
Accepted as CIP to
"Display Media…"

"Optically Written Display"
(Jason Eichenholz, M. Bass and Alexandra Rapaport)

Submitted 12/24/01

BIBLIOGRAPHY

[1] R. W. Boyd, "Nonlinear Optics", Academic Press, Inc. (1992).

[2] A. Rapaport, F. Szipocs, J. Milliez, H. Jenssen, M. Bass, K. Schafer, K. Belfield, "Optically written displays based on up-conversion of near infrared light", 20th International Display Research Conference, Palm Beach, Florida, USA (2000).

[3] Rapaport, F. Szipocs, J. Milliez, H. Jenssen, M. Bass, K. Schafer, K. Belfield, "Optically written displays based on up-conversion of near infrared light", IDW'00, Kobe, Japan (2000).

[4] X. X. Zhang, M. Bass, B. H. T. Chai, R. E. Peale, "Comparison of Yb, Ho up-conversion energy transfer in Different fluoride crystals", Advanced Solid-State Lasers, New Orleans, Louisiana, USA (1993).

[5] X. X. Zhang, P. Hong, M. Bass, R. E. Peale, H. Weidner, B. H. T. Chai, "Temperature and concentration dependence's of Ho^{3+} to Yb^{3+} energy transfer in Yb^{3+}, Ho^{3+} codoped KYF_4", *J. of Lumin.*, 60&61, pp. 878-881 (1994).

[6] X. X. Zhang, P. Hong, M. Bass, B. H. T. Chai, "Blue upconversion with excitation into Tm ions at 780 nm in Yb- and Tm-codoped fluoride crystals", *Phys. Rev. B*, **51**, No. 14, pp. 9298-9301 (1995).

[7] G. D. Gilliland, R. C. Powell, L. Esterowitz, "Spectral and up-conversion dynamics and their relationship to the laser properties of $BaYb_2F_8$:Ho^{3+}", *Phys. Rev. B*, **38**, No. 14, pp. 9958-9973 (1988).

[8] "Display media using passive hosts in which visible light emitting particulates excited by two photon absorption of one or two different frequency optical pump sources are dispersed" (M. Bass and H. Jennsen) U.S. Patent No.	Submitted 10/2/98 Prov. app.10/22/98 Full app. 11/24/99 Claims allowed 9/01 Issued
"Stabilized Luminescent Polymer Composition" (M. Bass and K. Belfield)	Submitted 8/2/2000 Accepted as CIP to "DisplayMedia…"
"Display media using passive hosts in which visible light emitting particulates excited by two photon absorption of one or two different frequency optical pump sources are dispersed" (M. Bass and H. Jennsen)	Submitted 12/15/00 Accepted as CIP to "Display Media…"